Topology optimization with finite-life fatigue constraints

Oest, Jacob; Lund, Erik

Published in:
Structural and Multidisciplinary Optimization

DOI (link to publication from Publisher):
10.1007/s00158-017-1701-9

Publication date:
2017

Document Version
Early version, also known as pre-print

Topology optimization with finite-life fatigue constraints

Jacob Oest*, Erik Lund†

Department of Materials and Production,
Aalborg University,
Fibigerstraede 16, 9220 Aalborg East, Denmark

Published in Structural and Multidisciplinary Optimization,
November 2017, Volume 56, Issue 5, pp 1045-1059

Abstract

This work investigates efficient topology optimization for finite-life high-cycle fatigue damage using a density approach and analytical gradients. To restrict the minimum mass problem to withstand a prescribed finite accumulated damage, constraints are formulated using Palmgren-Miner's linear damage hypothesis, S-N curves, and the Sines fatigue criterion. Utilizing aggregation functions and the accumulative nature of Palmgren-Miner's rule, an adjoint formulation is applied where the amount of adjoint problems that must be solved is independent of the amount of cycles in the load spectrum. Consequently, large load histories can be included directly in the optimization with minimal additional computational costs. The method is currently limited to proportional loading conditions and linear elastic material behavior and a quasi-static structural analysis, but can be applied to various equivalent stress-based fatigue criteria. Optimized designs are presented for benchmark examples and compared to stress optimized designs for static loads.

Keywords Topology optimization; Fatigue constraints; Adjoint method; P-norm

1 Introduction

In topology optimization the goal is to find an optimal material distribution within a prescribed design domain. Typically, the design domain is discretized using the finite element method, where each finite element is assigned a discrete value of 0 or 1 corresponding to void or solid material, respectively. However, such discrete programming problems with a large number of design variables are difficult to solve. Thus, the material distribution is often formulated in terms of a continuous function spanning from 0 to 1. As a result, more effective mathematical programming methods can be applied.

The continuous topology formulation presents a new problem, i.e. how to determine the structural response for intermediate densities. To address this, several methods have been applied [1–4]. In this work, the Solid Isotropic Material with Penalization (SIMP) method is used. The basic idea in SIMP is to penalize the stiffness for intermediate densities in such a manner, that the intermediate densities give a very low stiffness compared to the mass. The SIMP method is easy to implement in a finite element program [5, 6], and for certain relationships between the Poisson's ratio and the penalization power, the SIMP method presents real microstructural based models [7].

Topology optimization has been applied to a variety of fields, but most work has been done on minimizing the compliance under overall volume constraints. A stiffness optimal design provides much insight into the design as it presents optimal load paths. However, stiffness optimal designs often require major design alterations to fit more common design driving criteria such as stress or fatigue. Consequently, it can be very beneficial to introduce stress or fatigue criteria in the topology optimization formulation.

Stress-constrained structural optimization is an old research field. Some of the earliest work was done on single load truss design [8] and multi load truss design [9]. Sved and Ginos found that the global optimum to their three-bar truss design was a two-bar solution. However, the global optimum was unreachable by a gradient-based method because the stress constraint prevented the third bar from vanishing. This phenomenon, which also applies to topology optimization, is normally referred to as singular optima. These singular optima have been studied, and it has been shown that the singular optima belong to degenerate subspaces that are unreachable by standard non-linear programming techniques [10].

The issue with singular optima is normally addressed by relaxation techniques, where an alternative optimization problem is solved. Generally speaking, two types of relaxation techniques exist, where many variations thereof have been proposed. The two types of relaxation techniques are (i) the ε-relaxation technique [11], and (ii) the qp-approach [12]. In this work, the qp-based relaxed stress method as formulated by [13] is used. The basic idea is to expand the design space while also making intermediate densities yield very high stresses.

In stress-constrained topology optimization, it is common practice to evaluate the stress in at least one point in each finite element. Consequently, the number of con-

*✉ oest@m-tech.aau.dk
†✉ el@m-tech.aau.dk

straints is either equal to or higher than the number of design variables. For this reason, the benefit of using an adjoint formulation disappears, and as a consequence, the computational cost of the design sensitivity analysis is high. The two most common methods of dealing with the large number of constraints are active set strategies [14, 15] and constraint aggregation. In an active set strategy, a scheme is introduced to only include the most important constraints in the optimization. In constraint aggregation, several (or all) constraints are grouped together into an approximation of the constraints. Several different aggregation functions exist, e.g. the Kreisselmeier-Steinhauser function [16–20] and the P-norm function [13, 21]. Using aggregation functions is effective, but the local control is lost, and the optimization problem becomes increasingly non-linear. Furthermore, the aggregation functions are only approximations of the real constraint functions. Note that aggregation functions and active set strategies can be combined effectively. Recently, a method which addresses both the singular optima and the large number of stress constraints simultaneously has been proposed [22].

While structural optimization with stress constraints is an old field of research, fatigue constrained optimization is a relatively new and unexplored area. This can partly be explained by the high computational cost when having large load series. In an optimization setting this is both difficult to solve and computationally expensive. Furthermore, fatigue constrained optimization is a highly non-linear problem, and in a topology setting also suffers from the issues caused by vanishing constraints. However, the fact remains that fatigue is one of the most common failure modes in many engineering applications. Consequently, fatigue optimization is a steadily growing research field, where much interesting work has been done on shape optimization [23–25].

Fatigue constrained topology optimization has been addressed in a variety of ways. [26] addressed the dynamical nature of the loading conditions in their topology optimization by applying equivalent static loads [27,28]. The contribution by [29] incorporated dynamic fatigue and static failure criteria under constant and proportional loading. [30] utilized a modified Goodman failure criterion based on the Sines method to provide infinite-life design using topology optimization.

[31] applied fatigue constraints in their optimization where they decouple the fatigue analysis and topology optimization. A critical allowable fatigue stress is determined prior to the optimization by a design independent fatigue analysis, and then the minimum mass topology optimization is constrained by this allowable critical stress. The critical stress is determined using a predefined stress cycle history, Palmgren-Miner's accumulation rule and Haigh diagrams. By decoupling the fatigue analysis, the finite-life fatigue optimization can be solved as a static stress-constrained optimization. Thus, they optimize for a max principal stress constraint while also including a von Mises yield stress constraint. In [32] the idea of including the entire fatigue analysis directly in the optimization is given, but it was never realized.

In this work, a method that includes the quasi-static fatigue modeling directly in the topology optimization is applied. The approach is limited to proportional loading conditions and linear elastic material behavior. The fatigue is modeled using the Sines method which includes both amplitude and mean stress contributions. Additionally, the Sines method takes into account all stress components directly in the fatigue calculation. However, Sines method can easily be replaced with other multiaxial equivalent stress-based fatigue criteria in the approach. The amplitude and mean stress values used for the chosen fatigue criteria are determined using traditional rainflow-counting, i.e. the fatigue analysis thus follows standard practice for fatigue assessment and introduces no additional simplifications in the analysis. By including Palmgren-Miner's accumulation rule directly in the optimization constraint, no additional adjoint equations in the sensitivity analysis need to be solved for additional loads. A linear log-log S-N relationship is applied using Basquin's equation. However, the method is not limited to linear S-N curves. The method can be applied to 3D problems with the above assumptions. Lastly, it should be mentioned that the patent application by [33] describes some of the elements that are also presented in this paper.

The layout of the paper is as follows. In section 2 the analysis in the topology setting is presented, i.e. the material interpolation, the filtering techniques, and the applied P-norm function. In section 3 the fatigue analysis is presented. This includes the accumulation rule, the rainflow-counting, the S-N approximation, the fatigue criterion, and the adaptive constraint scaling scheme applied to the aggregation function. In section 4 the design sensitivity is presented for both stress-constrained optimization and the proposed formulation of fatigue-constrained optimization. More details on the design sensitivity analysis of the fatigue constraint is given in the appendix, where it can be seen, that implementing the fatigue constraint does not require much more effort than implementing a typical stress constraint. In section 5 the stress and fatigue optimization problems are presented, and benchmark examples are evaluated with different loading conditions in section 6. In section 7 the computational stability is discussed. Section 8 gives conclusive remarks on the method and presented results.

2 Structural setup

The aim of the optimization is to reduce overall mass by finding a (local) optimal material distribution that satisfies finite-life fatigue constraints. For sake of comparison, we also solve the minimization of mass constrained by a static von Mises stress criterion.

2.1 Material interpolation

The design domain is modeled by linear elastic finite element theory using four-node bilinear rectangular plane elements. Following the classical density-based approach [2, 3], each finite element e is assigned a density variable x_e. This density variable directly influences each elements Young's modulus of elasticity E_e. To calculate the Young's modulus for all possible densities the modified SIMP method is applied. The modified SIMP interpolates the modulus of elasticity by:

$$E_e\left(\tilde{x}_e\left(\boldsymbol{x}\right)\right) = E_{min} + \tilde{x}_e(\boldsymbol{x})^p \left(E_0 - E_{min}\right), \quad \forall e, \quad \boldsymbol{x} \in [0;1] \tag{1}$$

Here E_0 is the Young's modulus of the material, and $E_{min} \ll E_0$ is a lower bound on the modulus, representing the material stiffness of a void region. In this work $E_{min} = E_0 \cdot 10^{-6}$. p is a penalization factor set to $p = 3$ following common practice. $\tilde{x}_e$ is the filtered design variable described in section 2.2. The non-zero lower bound on the Young's modulus of elasticity is introduced to avoid a singular stiffness matrix. In this work linear elastic and isotropic material behavior is assumed.

2.2 Density filtering

Density filtering is applied to the design variables [34, 35] to avoid the so-called checkerboard patterns [36–38], which present an artificial high stiffness of the model. The density filter alters the design variables by including a weighted average of the densities of neighboring elements. The density filter for a given element e alters the density by:

$$\tilde{x}_e = \frac{\sum_{j \in \mathbb{N}_e} \omega\left(\mathbf{x}_j\right) x_j}{\sum_{j \in \mathbb{N}_e} \omega\left(\mathbf{x}_j\right)} \tag{2}$$

Here the set $\mathbb{N}_e$ includes the neighboring elements within a user-specified filter radius r relative to the center of element e. ω is a linearly decaying weight factor given by:

$$\omega\left(\mathbf{x}_j\right) = 1 - \frac{\left\|\mathbf{x}_j - \mathbf{x}_e\right\|}{r} \tag{3}$$

Here $\mathbf{x}_j$ and $\mathbf{x}_e$ are vectors containing the coordinates of the centroid of element j and e, respectively. The filtered densities $\tilde{\boldsymbol{x}}$ are henceforth referred to as physical variables as they enter directly into the physical model of the problem. In this framework, it means that the physical variables are used to compute the stiffness, to determine the overall mass of the structure, and to interpolate the stresses.

2.3 Finite element analysis

The structures are subjected to a time-varying load assumed independent of design. Due to the linear elastic modeling assumptions of the quasi-static analysis, the structural response is evaluated for a reference load $\hat{P}$ and then the structural response for all remaining time-steps can be found by linear superposition. The vector of global reference displacements $\hat{\boldsymbol{u}}$ caused by the reference load vector $\hat{\boldsymbol{P}}$ is found by solving the equilibrium state equation:

$$\boldsymbol{K}\left(\tilde{\boldsymbol{x}}\left(\boldsymbol{x}\right)\right)\hat{\boldsymbol{u}} = \hat{\boldsymbol{P}} \tag{4}$$

Here $\boldsymbol{K}$ is the interpolated global stiffness matrix. In this framework, all elements are of equal size and material type, thus only one pre-computed reference element stiffness matrix $\hat{\boldsymbol{K}}$ using a constitutive matrix with Young's modulus of unity needs to be calculated. Thus the global stiffness matrix can be constructed efficiently using the reference element stiffness matrix which is interpolated using the modified SIMP method:

$$\boldsymbol{K}\left(\tilde{\boldsymbol{x}}\left(\boldsymbol{x}\right)\right) = \sum_{e=1}^{n_e} E_e\left(\tilde{x}_e\left(\boldsymbol{x}\right)\right)\hat{\boldsymbol{K}} \tag{5}$$

For linear elastic conditions without pre-stress, the reference element stress $\hat{\boldsymbol{\sigma}}_e$ caused by the reference load can be found by:

$$\hat{\boldsymbol{\sigma}}_e = \tilde{x}_e(\boldsymbol{x})^q \boldsymbol{E}\boldsymbol{B}\hat{\boldsymbol{u}}_e \tag{6}$$

Here $\boldsymbol{E}$ is the constitutive matrix for full material density, $\boldsymbol{B}$ is the strain-displacement matrix and the exponent $q < 1$ is introduced to address the singularity phenomena by relaxing the design space. As with the reference element stiffness matrix, the constitutive matrix and the strain-displacement matrix can be pre-computed just once. In this work, the element stresses are evaluated at the superconvergent center point of each element.

The relaxed von Mises stress $\bar{\sigma}_e$ for element e caused by the reference load can be written as:

$$\bar{\sigma}_e = \sqrt{\hat{\sigma}_{e_x}^2 + \hat{\sigma}_{e_y}^2 - \hat{\sigma}_{e_x}\hat{\sigma}_{e_y} + 3\hat{\tau}_e^2} \tag{7}$$

Here $\hat{\sigma}_{e_x}$ and $\hat{\sigma}_{e_y}$ are the relaxed normal stress components in element e in the x- and y-direction, respectively. Likewise, $\hat{\tau}_e$ is the relaxed shear stress.

Due to the local nature of the stresses, each element constitutes a stress constraint in the optimization. For a fine discretization of the design domain this results in a very large number of constraints which may prove very computational demanding. For this reason, reducing the amount of constraints can be very beneficial. In the present work the P-norm function has been applied, where all constraints are grouped into a global constraint. The stress constraint g_σ is thus given by:

$$g_\sigma = \bar{\sigma}_{PN}\left(\tilde{\boldsymbol{x}}\left(\boldsymbol{x}\right)\right) = \left(\sum_{e=1}^{n_e} \left(\bar{\sigma}_e\left(\tilde{x}_e\left(\boldsymbol{x}\right)\right)\right)^P\right)^{\frac{1}{P}} \leq \sigma_y \tag{8}$$

Here the P-norm factor P should be a number $P > 1$ and σ_y is the material yield strength. The larger the P-norm factor, the closer the approximation will be to the highest value of all element stresses, henceforth noted $\bar{\sigma}_{max}$. On the other hand, a low number will present a very conservative estimate of the stresses. Having only one global P-norm function to represent the entire design domain can be a crude approximation, and it has previously been shown that better designs may be obtained by increasing the amount of aggregated global constraints in a given design domain. In the present work, the number of P-norm functions can easily be increased to achieve better approximations of the local constraints. However, this has not been a focus area in this work, and we instead refer to the published literature on the subject (e.g. [18, 39, 40]).

2.4 Objective function

The objective is to reduce overall mass. In this work the objective function $f(\boldsymbol{x})$ has been normalized to unity and is given by:

$$f\left(\boldsymbol{x}\right) = \frac{1}{n_e}\sum_{e=1}^{n_e} \tilde{x}_e\left(\boldsymbol{x}\right) \tag{9}$$

While most real industrial components have much more complex cost functions, the above cost function serves the purpose to find the lightest design only. Thus, the applied cost function is not representative of the production cost of a design.

3 Fatigue failure

Structures subjected to cyclic loading are prone to fail due to fatigue. To estimate the lifetime of a structure can be a complicated process. The designer must estimate the loading conditions, obtain material parameters based on tests, calculate the fractions of damage caused by each load cycle using an appropriate fatigue damage criterion, and sum up all the fractions of damage to estimate the accumulated damage. While fatigue analysis is not the main focus area of this article, we will briefly discuss these concepts as they have been applied in this framework. In this work, the fatigue damage is calculated using the multiaxial, stress-based Sines criterion, where the amplitude and mean stress values are found using traditional rainflow-counting. The damage is accumulated using Palmgren-Miner's rule, where the estimated cycles to failure have been calculated using a linear log-log S-N curve.

3.1 Rainflow-counting method

Assuming that the designer either knows or can estimate the stress spectrum for the entire lifetime, this spectrum can be reduced into stress reversals, also referred to as stress cycles. These cycles, along with their respective mean values, can be directly applied to Sines method to estimate the damage.

Various methods for determining the stress cycles exist, but the most popular method is the rainflow-counting method. In rainflow-counting, the full stress history is first reduced to peaks and valleys, and secondly half and full stress cycles are identified from these peaks and valleys. Due to the proportional loading condition, this can be done directly on the applied time-varying load. The concept is demonstrated in a small example for a sinusoidal load with increasing amplitude in Fig. 1. From the rainflow-counting on this example, $n_{RF} = 5$ different cycles are identified. The amount of reversals n_i, the amplitude scaling factor c_{a_i}, and the mean scaling factor c_{m_i} are obtained for all stress cycles $i = 1, \ldots, n_{RF}$. Note that the amplitude scaling factor is always positive in sign, while the mean scaling factor can be negative for compressive mean stress. The amplitude and mean stress vector for element e and cycle i can be determined by:

$$\begin{aligned} \boldsymbol{\sigma}_{e_{a,i}} &= c_{a_i}\hat{\boldsymbol{\sigma}}_e, \quad \forall e, i \\ \boldsymbol{\sigma}_{e_{m,i}} &= c_{m_i}\hat{\boldsymbol{\sigma}}_e, \quad \forall e, i \end{aligned} \tag{10}$$

The subscript a refers to amplitudes and the subscript m refers to mean. In a similar manner, the amplitude and mean element displacements can be determined. Note that the amplitude and mean stresses have not been binned in this work. In practical applications, this is often the case, since it reduces the computational costs of the analysis by limiting the amount of different cycles n_{RF} to a predefined number.

3.2 Fatigue damage by Sines method

[41] studied experimental data for combined bending and torsional loading of metals. He proposed that the alternating octahedral shear stress and the hydrostatic mean stress can be used as a multiaxial fatigue criterion for proportional loading of metals. In terms of alternating stress components, the criterion in a 2D plane stress and finite-life regime can be expressed as [42]:

$$\begin{aligned} \sqrt{\left(\sigma_{e_{ax,i}} - \sigma_{e_{ay,i}}\right)^2 + \sigma_{e_{ax,i}}^2 + \sigma_{e_{ay,i}}^2 + 6\tau_{e_{a,i}}^2} + \\ \beta(\sigma_{e_{mx,i}} + \sigma_{e_{my,i}}) = \sqrt{2}\tilde{\sigma}_{e_i} \end{aligned} \tag{11}$$

Here $\tilde{\sigma}_{e_i}$ is an equivalent uniaxial stress for element e and stress cycle i, and β is a material parameter. In absence of test data $\beta = 0.5$ is recommended [42], which is also the applied value in this work. Note that the damaging effects of a mean tensile stress in one direction can be reduced by a mean compressive stress in the other direction. It is assumed that a negative equivalent uniaxial stress state does not contribute to the overall fatigue damage. This common assumption makes the Sines criterion non-differentiable, but no special technique is applied to circumvent this.

The equivalent uniaxial stress $\tilde{\sigma}_{e_i}$ can be related to an estimated amount of cycles to failure N_{e_i} for that specific stress state using Basquin's equation. Basquin's equation represents a log-log straight line S-N relationship. Expressed in stress reversals, the S-N curve is given by:

$$\tilde{\sigma}_{e_i} = \sigma_f^{'}(2N_{ei})^b, \quad \forall e, i \tag{12}$$

Here $\sigma_f^{'}$ is the fatigue strength coefficient and b is the fatigue strength exponent, corresponding to the slope of the log-log S-N curve. This material-specific equation adds a very large non-linearity to the analysis. As previously mentioned, more complicated S-N curves can be applied. However, special care must be taken with materials with endurance limits. The sensitivities of damage for stress amplitudes below the endurance limit will be zero. This will hinder the optimizer in removing material in low damage regions. One way to overcome this issue is by introducing a very small slope on the endurance limit.

3.3 Damage accumulation

When the estimated amount of cycles to failure for a given alternating stress state is found, it is possible to apply Palmgren-Miner's linear damage hypothesis to accumulate the damage for the entire load spectrum. The accumulated fatigue damage in element e, D_e, is found by collecting all the fractions of damage D_{e_i} caused by each load cycle i:

$$D_e = c_D \sum_{i=1}^{n_{RF}} D_{e_i} = c_D \sum_{i=1}^{n_{RF}} \frac{n_i}{N_{ei}} \leq \eta, \quad \forall e \tag{13}$$

The upper limit describing when fatigue failure occurs is set to $\eta = 1$. c_D is a scaling parameter making the load history representative of the entire lifetime, thus $c_D \geq 1$. Applying the P-norm method, a global fatigue constraint g_D is found:

$$g_D = \left(\sum_{e=1}^{n_e} (D_e)^P\right)^{\frac{1}{P}} \leq \eta \tag{14}$$

Because of the highly nonlinear behavior of the S-N curve shown in (12), a logarithmic function with a base number of 10 has been applied to the constraint equation. This manipulation of numbers can improve convergence. For ease of notation, this is not included in the sensitivity analysis.

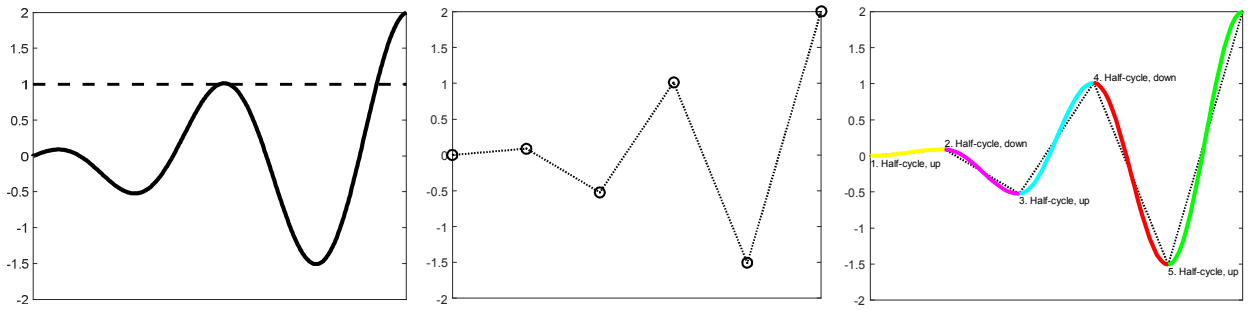

(a) (b) (c)

Figure 1: Rainflow-counting method. (a) Loading history in solid line and static reference load in dashed line. (b) Extrema found from history. (c) Cycles extracted from extrema, yielding scaling factors for amplitude c_a and mean c_m.

3.4 Adaptive constraint scaling method

A high P-norm factor is desirable to approximate the maximum function value, but it makes the optimization problem increasingly non-linear and thus even more difficult to solve. [13] proposed an adaptive constraint scaling scheme to scale the approximations towards the true local stress level. Using this method, one can achieve good designs using lower P-norm values, which in turn makes the optimization problem much easier to solve. For the global stress constrained problem it can be described by:

$$\bar{\sigma}_{max}^{(I)} \approx c^{(I)} \bar{\sigma}_{PN}^{(I)} \tag{15}$$

Here $g_\sigma = \bar{\sigma}_{PN}$ is replaced by the scaled approximation $\bar{\sigma}_{max}^{(I)}$ at each iteration (I). The approximation is determined using the adaptive constraint scaling factor $c^{(I)}$. For more details we refer to [13]. In Fig. 2 a pseudo algorithm for the implementation of the scheme is given, demonstrated on stress constraints. In order to include the influence of the adaptive constraint scaling scheme correctly in the design sensitivity analysis, the scaling factor $c^{(I)}$ must at least be once continuously differentiable. However, the scaling factor is assumed design independent in this work. The influence of this becomes less during the optimization as the scaling factor goes towards a constant near optimum, as pointed out in [13]. Note that the same adaptive constraint scaling scheme is used in the fatigue constrained optimization.

if Iteration $I \leq 2$ **then**
  $c^{(I)} = \frac{\bar{\sigma}_{max}^{(I)}}{\bar{\sigma}_{PN}^{(I)}}$
  $\alpha^{(I)} = 1$
else
  if oscillation **then**
    $\alpha^{(I)} = \max\left(0.5, \alpha^{(I-1)} \cdot 0.8\right)$
  else
    $\alpha^{(I)} = \min\left(1, \alpha^{(I-1)} \cdot 1.2\right)$
  end if
  $c^{(I)} = \alpha^{(I)} \frac{\bar{\sigma}_{max}^{(I-1)}}{\bar{\sigma}_{PN}^{(I-1)}} + \left(1 - \alpha^{(I)}\right) c^{(I-1)}$
end if

Figure 2: Pseudo code detailing the application of the adaptive constraint scaling scheme by [13]. The same scheme is applied in the fatigue optimization.

4 Design Sensitivity Analysis

In this section, the design sensitivity of the density filter, the cost function, the von Mises constraint, and the fatigue constraint is presented. As the stress constraint sensitivity is not an innovation of this work, it will only be stated and not derived. In the appendix, more details on the analytical sensitivity analysis of the fatigue constraint are given, where it can be seen that the sensitivity of the fatigue constraint is very similar to that of the stress constraint. Consequently, it does not require much additional work to implement. Throughout this paper, numerator-layout notation is used.

4.1 Design sensitivity of density filter

Using the chain rule of differentiation, the sensitivity of a function of the design variables, e.g. the cost function f, with respect to a change in a design variable x_e is:

$$\frac{df}{dx_e} = \sum_{j \in \mathbb{N}_e} \frac{df}{d\tilde{x}_j} \frac{d\tilde{x}_j}{dx_e} \tag{16}$$

Here the derivative of the physical design variable is given by:

$$\frac{d\tilde{x}_j}{dx_e} = \frac{\omega(\mathbf{x}_e)}{\sum_{k \in \mathbb{N}_j} \omega(\mathbf{x}_k)} \tag{17}$$

Note that this sensitivity is independent of the density and can thus be pre-computed to increase computational efficiency of the optimization. Note that a similar chain rule as shown in (16) is also applied to the constraint functions.

4.2 Cost function sensitivity

The cost function defined in (9) is an explicit function of the physical densities. Differentiating with respect to a physical design variable $\tilde{x}_j$ the sensitivity is given by:

$$\frac{df}{d\tilde{x}_j} = \frac{1}{n_e} \tag{18}$$

4.3 Stress constraint sensitivity

Since only a single global stress constraint is applied, and there are many design variables, the adjoint method can effectively be used to determine the design sensitivity of the aggregated von Mises stress constraint function. The sensitivity is obtained as:

$$\frac{dg_\sigma}{d\tilde{x}_j} = \frac{\partial g_\sigma}{\partial \tilde{x}_j} - \boldsymbol{\lambda}^T \frac{d\boldsymbol{K}}{d\tilde{x}_j}\hat{\boldsymbol{u}}, \qquad \forall j \tag{19}$$

Here the adjoint vector $\boldsymbol{\lambda}$ is found by solving the following adjoint equation:

$$\boldsymbol{K}\boldsymbol{\lambda} = \frac{\partial g_\sigma}{\partial \hat{\boldsymbol{u}}}^T \tag{20}$$

4.4 Fatigue constraint sensitivity

The fatigue constraint defined in (14) is an implicit function. The sensitivity is found using the adjoint method. It has previously been shown that using the adjoint method for multiple load cases can be effective [43, 44]. In the adjoint method an augmented constraint function $\check{g}_D$ is constructed by subtracting a zero-term from the original constraint function g_D. Thus, the augmented fatigue constraint $\check{g}_D$ can be written as:

$$\check{g}_D = g_D - \sum_{i=1}^{n_{RF}} \left(\boldsymbol{\lambda}_{a_i}^T \left(\boldsymbol{K}\boldsymbol{u}_{a_i} - \boldsymbol{P}_{a_i} \right) + \boldsymbol{\lambda}_{m_i}^T \left(\boldsymbol{K}\boldsymbol{u}_{m_i} - \boldsymbol{P}_{m_i} \right) \right) \tag{21}$$

Here $\boldsymbol{\lambda}_{a_i}$ and $\boldsymbol{\lambda}_{m_i}$ are the adjoint vectors corresponding to the amplitude and mean equilibrium. Utilizing the assumption that the loads are design independent, the sensitivity with respect to a physical design variable $\tilde{x}_j$ is given by:

$$\begin{aligned} \frac{d\check{g}_D}{d\tilde{x}_j} = \frac{\partial g_D}{\partial \tilde{x}_j} &- \sum_{i=1}^{n_{RF}} \left(\boldsymbol{\lambda}_{a_i}^T \frac{d\boldsymbol{K}}{d\tilde{x}_j}\boldsymbol{u}_{a_i} + \boldsymbol{\lambda}_{m_i}^T \frac{d\boldsymbol{K}}{d\tilde{x}_j}\boldsymbol{u}_{mi} \right) \\ &+ \sum_{i=1}^{n_{RF}} \left(\left(\frac{\partial g_D}{\partial \boldsymbol{u}_{ai}} - \boldsymbol{\lambda}_{a_i}^T \boldsymbol{K} \right) \frac{d\boldsymbol{u}_{a_i}}{d\tilde{x}_j} \right) \\ &+ \sum_{i=1}^{n_{RF}} \left(\left(\frac{\partial g_D}{\partial \boldsymbol{u}_{mi}} - \boldsymbol{\lambda}_{m_i}^T \boldsymbol{K} \right) \frac{d\boldsymbol{u}_{m_i}}{d\tilde{x}_j} \right), \qquad \forall j \end{aligned} \tag{22}$$

The computationally costly part of this equation is determining the Lagrange multipliers. Thus, it is desirable to eliminate the need for solving the adjoint equation for each stress cycle i.

Recalling the amplitude displacement $\boldsymbol{u}_{a_i}$ and mean displacement $\boldsymbol{u}_{m_i}$ can be found by scaling of the displacement $\hat{\boldsymbol{u}}$ caused by the reference load, they can be found by:

$$\begin{aligned} \boldsymbol{u}_{ai} &= c_{ai}\hat{\boldsymbol{u}}, \qquad \forall i \\ \boldsymbol{u}_{mi} &= c_{mi}\hat{\boldsymbol{u}}, \qquad \forall i \end{aligned} \tag{23}$$

Consequently, part of (22) can be rewritten:

$$\begin{aligned} \sum_{i=1}^{n_{RF}} \left(\boldsymbol{\lambda}_{a_i}^T \frac{d\boldsymbol{K}}{d\tilde{x}_j}\boldsymbol{u}_{a_i} + \boldsymbol{\lambda}_{m_i}^T \frac{d\boldsymbol{K}}{d\tilde{x}_j}\boldsymbol{u}_{mi} \right) = \\ \sum_{i=1}^{n_{RF}} \left(c_{ai}\boldsymbol{\lambda}_{a_i}^T + c_{m_i}\boldsymbol{\lambda}_{m_i}^T \right) \frac{d\boldsymbol{K}}{d\tilde{x}_j}\hat{\boldsymbol{u}} \end{aligned} \tag{24}$$

Thus, if the sum of all scaled Lagrange multipliers can be found efficiently, the sensitivity can be found efficiently. For ease of notation, this sum is defined as $\boldsymbol{\Lambda}$:

$$\boldsymbol{\Lambda} = \sum_{i=1}^{n_{RF}} \left(c_{ai}\boldsymbol{\lambda}_{a_i} + c_{m_i}\boldsymbol{\lambda}_{m_i} \right) \tag{25}$$

The derivative of the reference displacement is found by differentiating the equilibrium state equation defined in (4):

$$\boldsymbol{K}\frac{d\hat{\boldsymbol{u}}}{d\tilde{x}_j} = -\frac{d\boldsymbol{K}}{d\tilde{x}_j}\hat{\boldsymbol{u}} \tag{26}$$

The derivatives of the amplitude and mean displacement can be found by utilizing scaling of the reference displacement. Consequently, they can be written as:

$$\begin{aligned} \frac{d\boldsymbol{u}_{ai}}{d\tilde{x}_j} &= -c_{a_i}\boldsymbol{K}^{-1}\frac{d\boldsymbol{K}}{d\tilde{x}_j}\hat{\boldsymbol{u}} \\ \frac{d\boldsymbol{u}_{mi}}{d\tilde{x}_j} &= -c_{m_i}\boldsymbol{K}^{-1}\frac{d\boldsymbol{K}}{d\tilde{x}_j}\hat{\boldsymbol{u}} \end{aligned} \tag{27}$$

Using these equations, the adjoint problem can be altered. Thus (22) can be written as:

$$\begin{aligned} \frac{d\check{g}_D}{d\tilde{x}_j} = \frac{\partial g_D}{\partial \tilde{x}_j} - \boldsymbol{\Lambda}^T \frac{d\boldsymbol{K}}{d\tilde{x}_j}\hat{\boldsymbol{u}} + \sum_{i=1}^{n_{RF}} \Bigg[c_{a_i}\frac{\partial g_D}{\partial \boldsymbol{u}_{ai}} - c_{a_i}\boldsymbol{\lambda}_{a_i}^T\boldsymbol{K} \\ + c_{m_i}\frac{\partial g_D}{\partial \boldsymbol{u}_{mi}} - c_{m_i}\boldsymbol{\lambda}_{m_i}^T\boldsymbol{K} \Bigg] \left(-\boldsymbol{K}^{-1}\frac{d\boldsymbol{K}}{d\tilde{x}_j}\hat{\boldsymbol{u}} \right) \end{aligned} \tag{28}$$

The computational costly part of this equation is $\left(-\boldsymbol{K}^{-1}\frac{d\boldsymbol{K}}{d\tilde{x}_j}\hat{\boldsymbol{u}}\right)$. In fact, this is the computational costly part of the design sensitivity when using the direct differentiation method. Thus, $\boldsymbol{\Lambda}$ is selected to eliminate the expression within the square brackets, i.e.:

$$\boldsymbol{K}\boldsymbol{\Lambda} = \sum_{i=1}^{n_{RF}} \left(c_{a_i}\frac{\partial g_D}{\partial \boldsymbol{u}_{ai}}^T + c_{mi}\frac{\partial g_D}{\partial \boldsymbol{u}_{mi}}^T \right) \tag{29}$$

By this equation, the computational costs no longer scale poorly with the amount of load cycles. The derivative of the fatigue constraint is then obtained by (28) which has been reduced using the Lagrange multiplier $\boldsymbol{\Lambda}$:

$$\frac{d\check{g}_D}{d\tilde{x}_j} = \frac{\partial g_D}{\partial \tilde{x}_j} - \boldsymbol{\Lambda}^T \frac{d\boldsymbol{K}}{d\tilde{x}_j}\hat{\boldsymbol{u}} \tag{30}$$

With this formulation, very large load series can be applied without a significant increase to the computational demand. A more detailed description of the analytical sensitivity analysis can be found in the appendix.

Numerous fatigue criteria exist. Therefore it is advantageous to have a generic method which is not too specific for a certain fatigue criterion. Thus, it is important to stress that this sensitivity analysis can be applied to many different equivalent stress-based criteria. For other methods, different difficulties may be introduced. For instance, in critical plane methods the location of the critical plane and its sensitivities must be found.

As the adjoint vector only needs to be solved once per constraint per iteration, a semi-analytical approach can also be applied efficiently. Using semi-analytical approaches,

different fatigue criteria can be applied with very little implementation effort. Additionally, the amount of partial derivatives that must be calculated is directly dependent on the amount of stress cycles n_{RF}. Thus the computational effort can be further reduced by combining cycles into bins.

5 Problem definition

Two different optimization problems are solved in this framework. Minimization of mass with $\mathbb{P}_1$ a global von Mises static stress constraint, and $\mathbb{P}_2$ with a global fatigue constraint using a time-varying load. Written as optimization problems, they are

$$\mathbb{P}_1 \begin{cases} \min\limits_{\boldsymbol{x}\in\boldsymbol{X}} & f(\boldsymbol{x}) \\ \text{s.t.} & \frac{g_\sigma(\boldsymbol{x})}{\sigma_y} \leq 1 \end{cases}$$

$$\mathbb{P}_2 \begin{cases} \min\limits_{\boldsymbol{x}\in\boldsymbol{X}} & f(\boldsymbol{x}) \\ \text{s.t.} & \frac{g_D(\boldsymbol{x})}{\eta} \leq 1 \end{cases}$$

Here $\boldsymbol{X} = \{\boldsymbol{x} \in \mathbb{R}^e | \, 0 \leq x_e \leq 1, e = 1, \ldots, n_e\}$.

The optimization problems are solved using the Method of Moving Asymptotes (MMA) by [45]. Using the notation in the 2007 MATLAB implementation of MMA by Svanberg, the optimization problems that are solved can be written as [46]:

$$\begin{aligned} \min_{\boldsymbol{x}\in\boldsymbol{X},\boldsymbol{y}\geq\boldsymbol{0},z\geq 0} \quad & f_0(\boldsymbol{x}) + a_0 z + \sum_{l=1}^{n_l}\left(c_l y_l + \frac{1}{2} d_l y_l^2\right) \\ s.t. \quad & f_l(\boldsymbol{x}) - a_l z - y_l \leq 0, \quad l = 1, \ldots, n_l \end{aligned}$$

Here $n_l = 1$ is the number of general constraints. The MMA optimization problem is mentioned such that all applied parameters are clearly defined. All parameters not defined in this paper are left to the default values. Following parameters have been chosen:

$$\begin{aligned} a_0 &= 1 \\ a_l &= 0, \qquad \forall l \\ c_l &= 1000, \quad \forall l \\ d_l &= 1, \qquad \forall l \end{aligned}$$

To address the highly non-linear behavior of the optimization problem, the increase and decrease factors for the asymptotes have been reduced to 1.05 and 0.65, respectively. All examples are generated from an initial design where $x_e = 0.5, \forall e$, and all examples use a filter radius r of 1.5 times the element length.

As the two optimization problems behave differently, some optimization settings differ. The outer move limit ML is specified in each example. In the stress optimization, the stress penalization factor is set to $q = 0.50$, whereas a continuation scheme is applied for the fatigue optimization. In the continuation scheme, an initial value $q = 0.75$ is used, and this value is decreased by 0.01 every third iteration until $q = 0.50$. While this change in penalization is quite small, it has been observed to work well. The stiffness penalization factor $p = 3$ remains unchanged in both optimization formulations.

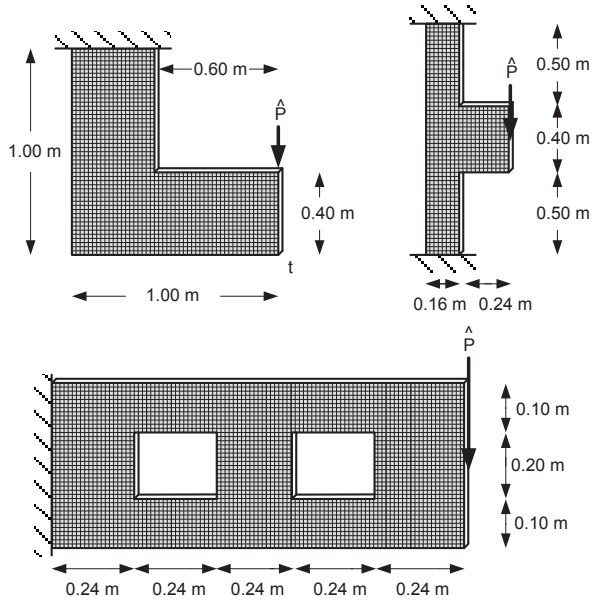

Figure 3: The L plate, the double-L plate and the cantilever plate.

The optimization problems are given a convergence criterion stating that if the relative change in design $\Delta\boldsymbol{x}^{(l)} = \left\|\boldsymbol{x}^{(l)} - \boldsymbol{x}^{(l-1)}\right\|$ is below a set threshold $\Delta\boldsymbol{x}_{min}$, the optimization is stopped. For the stress optimizations $\Delta\boldsymbol{x}_{min} = 0.150\%$ is used, and for the fatigue optimizations $\Delta\boldsymbol{x}_{min} = 0.075\%$ is used as the fatigue optimizations converge slower. Note that this convergence criterion does not guarantee feasibility.

6 Examples

Three different examples are solved and common for all is that the shapes give rise to stress concentrations. The first example is an L plate which is used to demonstrate a loading condition where a fatigue design similar to a von Mises stress constrained design is achieved. The second and third examples, a double-L plate and a cantilever plate with holes, are used to demonstrate designs that differ from a stress-optimized design. The three different structures are depicted on Fig. 3. All three plates have a thickness of $t = 0.02m$, and all examples make use of the default random number generator in MATLAB to determine the loads. More specifically, this is the Mersenne Twister pseudorandom number generator with a seed of 0. In all the results shown, the density plots are with the physical density variables while the stress and fatigue plots are with penalized values. For sake of comparison stress plots are also shown for the fatigue optimized designs subjected to the reference load. Likewise, fatigue plots are shown for the stress optimized designs subjected to the fatigue loading. Additionally, for each design the maximum normalized von Mises stress and the maximum fatigue damage are presented. The material applied is AISI 1020 HR steel. The material values, which are taken from [42], are presented in Table 1.

Table 1: Material properties of AISI 1020 HR.

$\sigma_f^{'} = 1,384\ MPa$	$E_0 = 203\ GPa$	$b = -0.156$
$\nu = 0.30$	$\sigma_y = 262\ MPa$	

6.1 Example I: L plate

A standard test benchmark example in stress constrained topology optimization is the L plate. The L plate suffers from high stress concentrations at the boundaries. However, the largest stress for a dense design is at the sharp corner. A stress or stress-based fatigue optimized design should avoid this stress concentration. Conventional stiffness optimized design will not avoid this stress concentration, and the L-bracket therefore constitutes a good example of a design where a stiffness optimal design will require large design alterations to suit a stress or fatigue constraint.

Two different optimizations are carried out. $\mathbb{P}_1$ subject to $\hat{P} = 50\ kN$ and $\mathbb{P}_2$ subject to $k = 1,000$ random loads defined by $P_k = rand(\hat{P}, -\hat{P}), \forall k$. It is assumed that the structure is subjected to the loading spectrum $c_D = 750$ times. c_D is tailored to give a fatigue optimized design with a similar volume fraction as the stress optimized design.

The design domain is discretized with $n_e = 6,400$ elements. The applied loads are distributed onto three elements consistently along the vertical edge to lessen the stress concentration at the loaded region. These three elements are excluded from the optimization and set to have a density of 1. Both optimizations have a P-norm factor of $P = 8$.

Since the loading in $\mathbb{P}_2$ is fully reversed, the two optimized designs resemble each other to a large extent. Due to the increase in non-linearity of the fatigue constraint, the stress constrained topology is obtained in fewer optimization iterations. While the fatigue optimized design is slightly heavier than the stress optimized design, the highest von Mises stress is also slightly lower than the material yield limit. The results are shown on Fig. 4 and in Table 2.

Both designs are nearly fully stressed. The fatigue optimized design also manages to have a large portion of the design fully damaged. However, fewer elements are damaged as compared to the number of fully stressed elements, which shows the large non-linearity and local behavior of this type of constraint.

Even though the stresses are almost equal in both designs, the slightly higher stresses in the stress optimized design causes the structure to fail due to fatigue damage. This clearly shows how sensitive fatigue damage is to very small variations in stresses.

6.2 Example II: Double-L plate

In this second example, a symmetric double-L plate clamped at each end is investigated. This design space resembles the L plate to a large extent, and the optimizations should attempt to avoid the stress concentrations at the two sharp edges.

The static reference load applied in $\mathbb{P}_1$ is $\hat{P} = 75\ kN$, distributed onto six elements at the vertical edge. In the fatigue optimization $\mathbb{P}_2$ the load spectrum contains $k = 1,000$ loads, and is defined by $P_k = rand(\hat{P}, -\hat{P}/2), \forall k$. The damage is scaled with $c_D = 10,000$.

Table 2: Optimization settings and results for example I

Optimization Settings

$\mathbb{P}_1$	$\mathbb{P}_2$
$ML = 20\%$	$ML = 5\%$
$\Delta \boldsymbol{x}_{min} = 0.15\%$	$\Delta \boldsymbol{x}_{min} = 0.075\%$
$n_e = 6,400$	
$P = 8$	

Optimization Results

$\mathbb{P}_1$	$\mathbb{P}_2$
$f = 0.2412$	$f = 0.2449$
$Iter = 330$	$Iter = 477$
$max(\bar{\sigma}_e/\sigma_y) = 1.0003$	$max(\bar{\sigma}_e/\sigma_y) = 0.9479$
$max(D_e) = 1.4319$	$max(D_e) = 1.0057$

In this problem, the design domain is discretized using a fine discretization of $n_e = 23,040$ and the aggregation function is assigned a high P-norm value of $P = 12$. The larger P value in this example is set to avoid poor local minima where only elements near the boundaries are fully stressed. The results are shown on Fig. 5 and in Table 3.

The von Mises constrained design produces a symmetric design that tries to avoid the stress concentrations at the edges. The stress optimized design fails to withstand the fatigue load at many elements, and the highest fatigue damage is more than eight times too high.

The fatigue constrained design is asymmetric. This is due to the difference in mean stress effects caused by the loading condition which is not fully reversed. In the upper part of the design, similar trends to the stress constrained design can be seen. Again, many elements are fully damaged. The fatigue optimized design successfully strengthens the regions where the stress optimized design fails. As expected, a large number of these elements have a relative low von Mises stress value for the reference load. The fatigue damage is sustained at a similar volume fraction as the stress optimized design, but with higher von Mises stresses for the reference load. The optimizer allows high stresses in low damage regions to fully damage the structure. These regions can easily be identified by the damage plot for the stress optimized design or by the stress plot in the fatigue optimized design.

6.3 Example III: Cantilever plate

In this example, two holes are introduced in a cantilever plate to give stress concentrations in the initial design. The domain is discretized using $n_e = 15,360$ elements. The reference load is $\hat{P} = 40\ kN$ and is consistently distributed onto six elements. In the fatigue optimization, $k = 1,000$ loads are defined by $P_k = rand(\hat{P}, -2\hat{P}/5), \forall k$. This loading is assumed to occur $c_D = 10,000$ times. With this loading condition, the fatigue constrained design will not be symmetric as regions subjected to high tensile stresses will dominate the design. The applied loading condition primarily gives

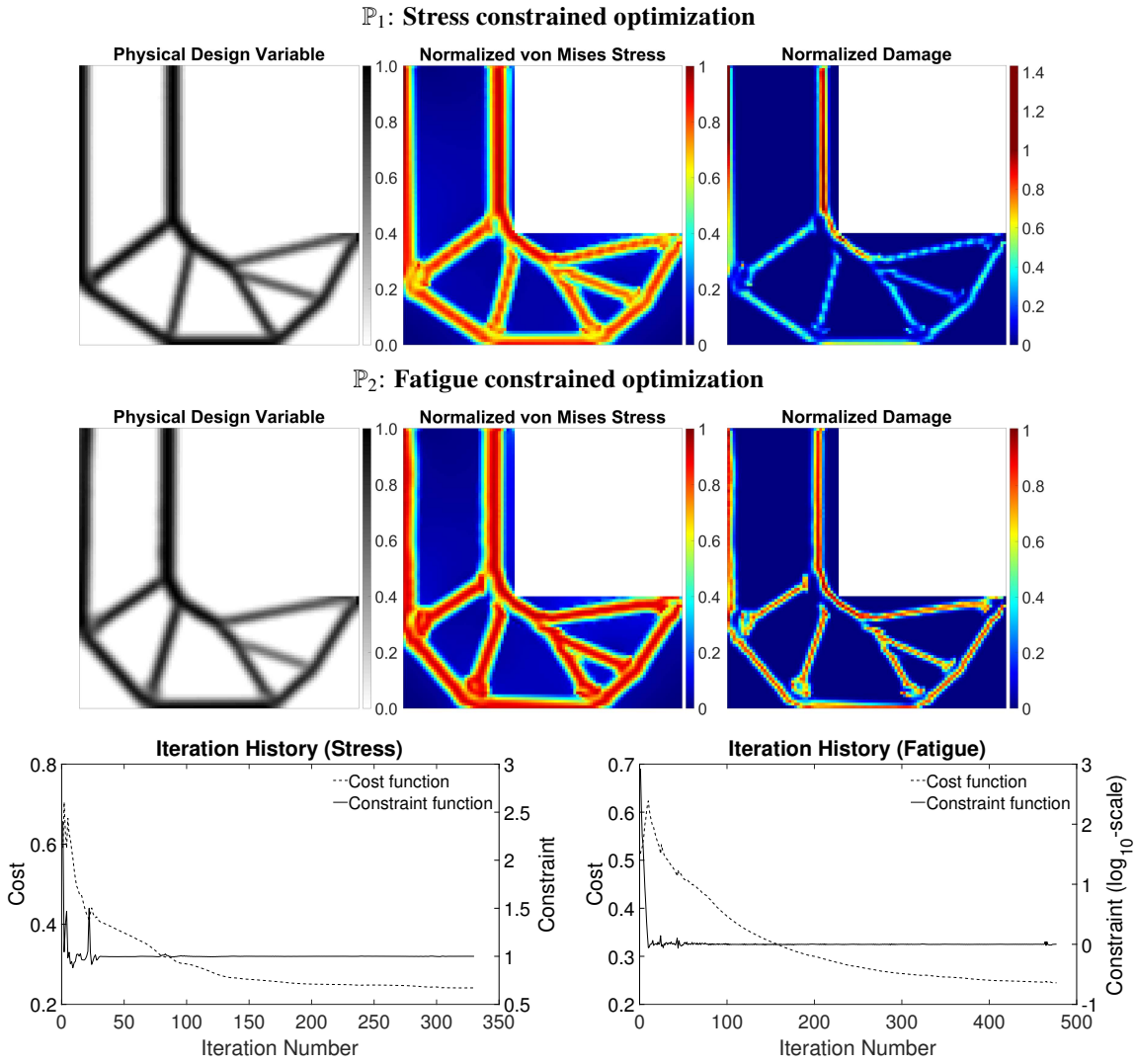

Figure 4: Optimization results of the L plate example. The stress values are normalized with respect to the yield stress $\sigma_y = 262\ MPa$, and the damage values are normalized with respect to the fatigue limit $\eta = 1$. Note that the normalized damage plot contains real function values, and all values above the allowable limit are assigned the same color code. Also note that the iteration history for fatigue is using the log_{10} scale.

Table 3: Optimization settings and results for example II

Optimization Settings

$\mathbb{P}_1$	$\mathbb{P}_2$
$ML = 10\%$	$ML = 5\%$
$\Delta \boldsymbol{x}_{min} = 0.15\%$	$\Delta \boldsymbol{x}_{min} = 0.075\%$
$n_e = 23,040$	
$P = 12$	

Optimization Results

$\mathbb{P}_1$	$\mathbb{P}_2$
$f = 0.2073$	$f = 0.2070$
$Iter = 262$	$Iter = 682$
$max(\bar{\sigma}_e/\sigma_y) = 0.9998$	$max(\bar{\sigma}_e/\sigma_y) = 1.1768$
$max(D_e) = 8.0851$	$max(D_e) = 0.9991$

compressive mean stresses in the lower part of the structure. As negative Sines equivalent stresses do not contribute to the overall damage, less damage is caused in the lower part of the structure. This trend is seen on Fig. 6, where it is clear that the top part of the beam, which is primarily subjected to tension, is thicker than the lower part of the beam. In other words, the fatigue optimized design is strengthened in regions where the stress optimized design has too high fatigue damage. The fatigue optimization also manages to remove an almost undamaged bar near the clamped boundary. The optimization settings and results are listed in Table 4.

7 Discussion

The fatigue constrained topology optimization is a difficult problem to solve. This is clear from the degree of infeasibility during optimization, and also from the amount of iterations required before convergence. In general, a sudden and large increase in the adaptive constraint scaling factor $c^{(l)}$ often causes problems. This rapid increase is caused by a poor representation by the P-norm function, caused by

$\mathbb{P}_1$: **Stress constrained optimization**

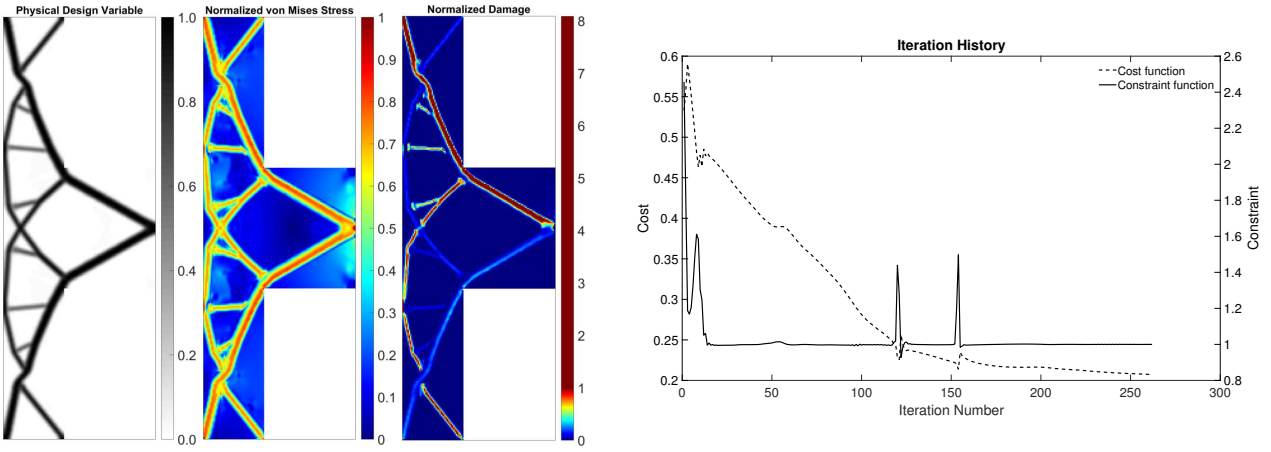

$\mathbb{P}_2$: **Fatigue constrained optimization**

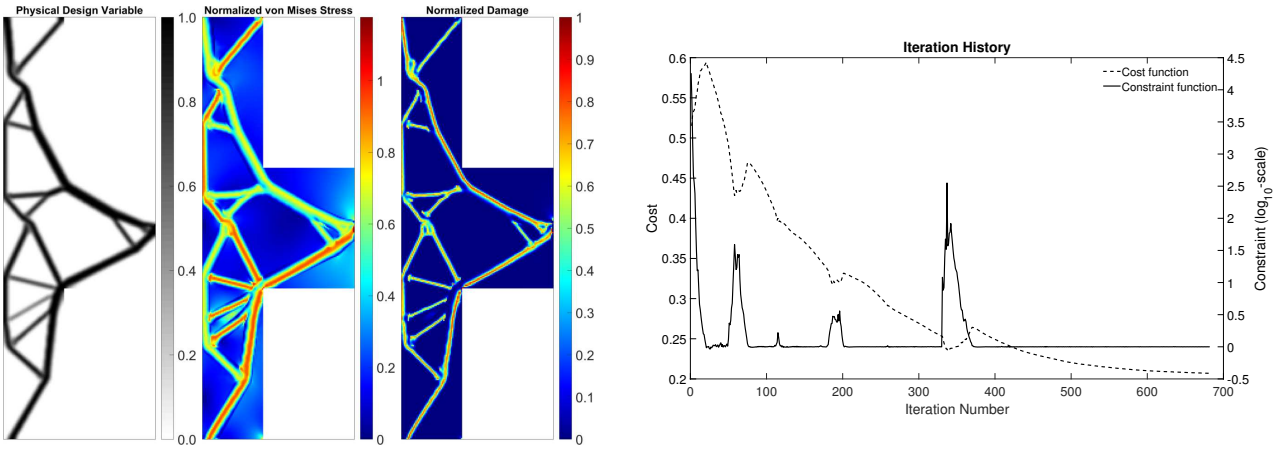

Figure 5: Optimization results of the double-L plate example. The stress values are normalized with respect to the yield stress $\sigma_y = 262\ MPa$, and the damage values are normalized with respect to the fatigue limit $\eta = 1$. Note that the normalized damage plot contains real function values, and all values above the allowable limit are assigned the same color code. Also note that the iteration history for fatigue is using the log_{10} scale.

Table 4: Optimization settings and results for example III

Optimization Settings

$\mathbb{P}_1$	$\mathbb{P}_2$
$ML = 15\%$	$ML = 5\%$
$\Delta \boldsymbol{x}_{min} = 0.15\%$	$\Delta \boldsymbol{x}_{min} = 0.075\%$
$n_e = 15,360$	
$P = 12$	

Optimization Results

$\mathbb{P}_1$	$\mathbb{P}_2$
$f = 0.2432$	$f = 0.2542$
$Iter = 246$	$Iter = 620$
$max(\bar{\sigma}_e/\sigma_y) = 0.9989$	$max(\bar{\sigma}_e/\sigma_y) = 1.1469$
$max(D_e) = 5.4933$	$max(D_e) = 0.9998$

large jumps in constraint function values. Thus, increasing the P-norm factor can be beneficial, but since the problem is already very non-linear, it can make the optimization unstable. A similarly ambivalent issue is the mesh resolution. A very fine mesh better captures the stress field and thus the fatigue damage, but increasing the number of finite elements in a P-norm function also lessens the accuracy of the P-norm.

It is advisable to start the fatigue optimization infeasible, as the damage behaves so non-linearly that an element with almost no damage can become very infeasible with very small design changes. This can cause problems if a design is far from failure and is allowed to have large design changes. However, if the move limit and optimizer settings are set to enforce small design changes, the optimization is quite stable. Lastly it must be noted that it can be difficult to obtain a completely black and white design, as can be observed in particular in example III.

All of the above observations may be problem specific, and very dependent on which fatigue criterion and S-N curve that is applied. During the verification of the implementation of the method, it was observed that finite difference approximations yield accurate sensitivities. As a result, a semi-analytical approach can be used effectively.

It must be stressed that dynamic effects are not included in the quasi-static analysis. Furthermore, some parameters that are well-known to influence fatigue are neglected. To name a few of these parameters, they could be sur-

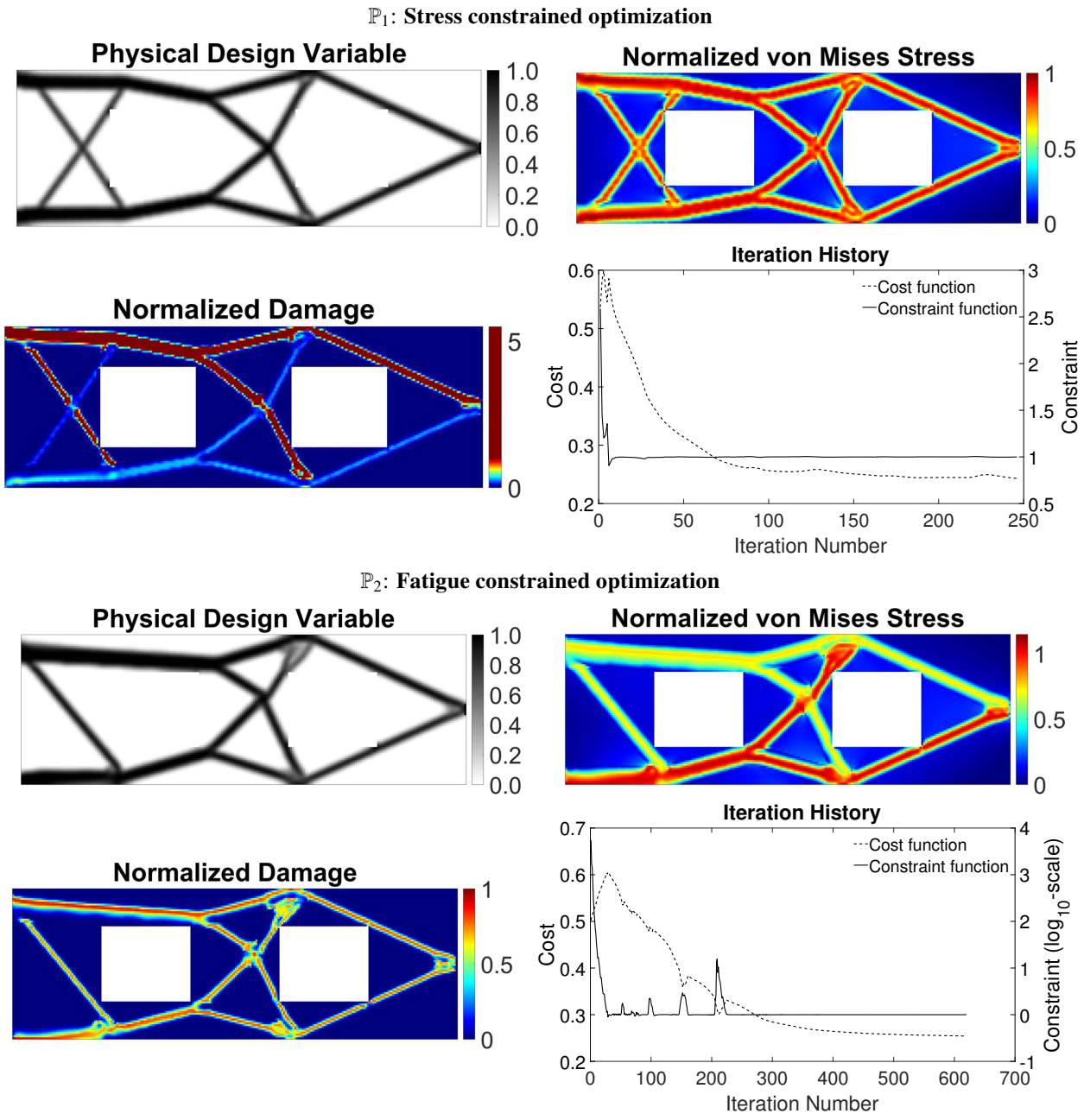

Figure 6: Optimization results of the cantilever plate example. The stress values are normalized with respect to the yield stress $\sigma_y = 262\ MPa$, and the damage values are normalized with respect to the fatigue limit $\eta = 1$. Note that the normalized damage plot contains real function values, and all values above the allowable limit are assigned the same color code. Also note that the iteration history for fatigue is using the log_{10} scale.

face treatments, temperature and environmental effects etc. Some of these effects can be included through appropriate S-N curves, while others cannot. Thus, it is important to have a profound knowledge of the optimization problem at hand and only use the presented method for preliminary design. For a detailed description of factors that can affect the fatigue properties and thus influence the optimization, see [31].

8 Conclusion

A general gradient-based method for finite-life fatigue optimization that includes the entire high-cycle fatigue analysis directly in the optimization has been presented. It is very effective for problems where rainflow-counting can be performed on the loading conditions, as only one adjoint vector per constraint equation has to be solved for every reference load vector. The method is not limited to 2D applications, and is generic in the sense that many different equivalent stress-based fatigue criteria can be applied. The method applies to linear finite element modeling with linear elastic material behavior.

The optimization problem is highly non-linear and more difficult to solve than classical stress-based optimization. An example was given, where a fatigue optimized design and a stress optimized design yielded similar results. This

is caused by the applied loading and the similarity in the Sines damage criterion and the von Mises stress criterion. Two examples where the fatigue optimized designs are different from stress optimized designs were also presented.

The proposed method does not require much more implementation work than typical stress-based topology optimization, and is of such a powerful preliminary-design tool for engineering problems driven by fatigue.

Acknowledgements

This research is part of the project ABYSS – Advancing BeYond Shallow waterS – Optimal design of offshore wind turbine support structures, sponsored by the Danish Council for Strategic Research, Grant no. 1305-00020B. This support is gratefully acknowledged.

Appendix

In the following the partial derivatives in the sensitivity analysis of the fatigue constraint is written using the chain rule of differentiation. The independence or linear dependence on the load scaling factors is indicated.

The partial derivative of the fatigue constraint with respect to a physical design variable $\tilde{x}_j$ can be written as:

$$\begin{aligned}\frac{\partial g_D}{\partial \tilde{x}_j} =& \frac{\partial g_D}{\partial D_j}\sum_{i=1}^{n_{RF}}\left(\frac{\partial D_{j_i}}{\partial N_{j_i}}\frac{\partial N_{j_i}}{\partial \tilde{\sigma}_{j_i}}\left(c_{a_i}\left(\frac{\partial \tilde{\sigma}_j}{\partial \hat{\sigma}_{j_x}}\frac{\partial \hat{\sigma}_{j_x}}{\partial \tilde{x}_j}+\right.\right.\right. \\ & \frac{\partial \tilde{\sigma}_j}{\partial \hat{\sigma}_{j_y}}\frac{\partial \hat{\sigma}_{j_y}}{\partial \tilde{x}_j}+\frac{\partial \tilde{\sigma}_j}{\partial \hat{\tau}_j}\frac{\partial \hat{\tau}_j}{\partial \tilde{x}_j}\Big)+ \\ & \left.\left.\left. c_{m_i}\left(\frac{\partial \tilde{\sigma}_j}{\partial \hat{\sigma}_{j_{mx}}}\frac{\partial \hat{\sigma}_{j_x}}{\partial \tilde{x}_j}+\frac{\partial \tilde{\sigma}_j}{\partial \hat{\sigma}_{j_{my}}}\frac{\partial \hat{\sigma}_{j_y}}{\partial \tilde{x}_j}\right)\right)\right)\end{aligned} \tag{31}$$

In this equation, the Sines stress differentiated with respect to the stress components and the stress components differentiated with respect to the physical design variables do not need to be calculated directly for each stress cycle i. Consequently, only the computational inexpensive partial derivatives $\partial D_{j_i}/\partial N_{j_i}$ and $\partial N_{j_i}/\partial \tilde{\sigma}_{j_i}$ need to be calculated for every load cycle.

The partial derivative of the aggregated constraint function with respect to the accumulated damage is given by:

$$\frac{\partial g_D}{\partial D_j} = \left(\sum_{e=1}^{n_e} D_e^P\right)^{\frac{1}{P}-1}\cdot D_j^{P-1} \tag{32}$$

The partial derivative of the damage with respect to the estimated amount of cycles to failure is:

$$\frac{\partial D_{j_i}}{\partial N_{j_i}} = -c_D\frac{n_{j_i}}{N_{j_i}^2} \tag{33}$$

The partial derivative of the estimated cycles to failure with respect to the Sines equivalent stress is:

$$\frac{\partial N_{j_i}}{\partial \tilde{\sigma}_{j_i}} = \frac{1}{2}\left(\frac{\left(\frac{\tilde{\sigma}_{j_i}}{\sigma_f'}\right)^b}{\tilde{\sigma}_{j_i}}\right) \tag{34}$$

The partial derivatives of the Sines equivalent stress are found by:

$$\frac{\partial \tilde{\sigma}_j}{\partial \hat{\sigma}_{j_x}} = \frac{1}{4}\frac{\left(4\hat{\sigma}_{j_x}-2\hat{\sigma}_{j_y}\right)\sqrt{2}}{\sqrt{\left(\hat{\sigma}_{j_x}-\hat{\sigma}_{j_y}\right)^2+\hat{\sigma}_{j_x}^2+\hat{\sigma}_{j_y}^2+6\hat{\tau}_j^2}} \tag{35}$$

$$\frac{\partial \tilde{\sigma}_j}{\partial \hat{\sigma}_{j_y}} = \frac{1}{4}\frac{\left(4\hat{\sigma}_{j_y}-2\hat{\sigma}_{j_x}\right)\sqrt{2}}{\sqrt{\left(\hat{\sigma}_{j_x}-\hat{\sigma}_{j_y}\right)^2+\hat{\sigma}_{j_x}^2+\hat{\sigma}_{j_y}^2+6\hat{\tau}_j^2}} \tag{36}$$

$$\frac{\partial \tilde{\sigma}_j}{\partial \hat{\tau}_j} = \frac{3\hat{\tau}_j\sqrt{2}}{\sqrt{\left(\hat{\sigma}_{j_x}-\hat{\sigma}_{j_y}\right)^2+\hat{\sigma}_{j_x}^2+\hat{\sigma}_{j_y}^2+6\hat{\tau}_j^2}} \tag{37}$$

$$\frac{\partial \tilde{\sigma}_j}{\partial \hat{\sigma}_{j_{mx}}} = \frac{\partial \tilde{\sigma}_j}{\partial \hat{\sigma}_{j_{my}}} = \frac{1}{2}\beta\ \sqrt{2} \tag{38}$$

Note that these values are unscaled and it is therefore not necessary to calculate these derivatives for each cycle i. Similarly, the stress components differentiated with respect to the physical design variables can be calculated independently of the cycles, i.e. without the scaling factors:

$$\frac{\partial \hat{\boldsymbol{\sigma}}_j}{\partial \tilde{x}_j} = \begin{bmatrix} \frac{\partial \hat{\sigma}_{j_x}}{\partial \tilde{x}_j} \\ \frac{\partial \hat{\sigma}_{j_y}}{\partial \tilde{x}_j} \\ \frac{\partial \hat{\tau}_j}{\partial \tilde{x}_j} \end{bmatrix} = q\tilde{x}_j(x)^{q-1}\boldsymbol{E}_j\boldsymbol{B}_j\hat{\boldsymbol{u}}_j \tag{39}$$

Likewise, the partial derivative of the constraint function with respect to the amplitude and mean displacement, that are required to solve the adjoint problem can be found by:

$$\begin{aligned}\frac{\partial g_D}{\partial \boldsymbol{u}_{j_a}} =& \frac{\partial g_D}{\partial D_j}\sum_{i=1}^{n_{RF}}\left(c_{a_i}\frac{\partial D_{j_i}}{\partial \tilde{\sigma_{j_i}}}\left(\frac{\partial \tilde{\sigma}_j}{\partial \hat{\sigma}_{j_x}}\frac{\partial \hat{\sigma}_{j_x}}{\partial \hat{\boldsymbol{u}}_j}+\right.\right. \\ & \left.\left.\frac{\partial \tilde{\sigma}_j}{\partial \hat{\sigma}_{j_y}}\frac{\partial \hat{\sigma}_{j_y}}{\partial \hat{\boldsymbol{u}}_j}+\frac{\partial \tilde{\sigma}_j}{\partial \hat{\tau}_j}\frac{\partial \hat{\tau}_j}{\partial \hat{\boldsymbol{u}}_j}\right)\right)\end{aligned} \tag{40}$$

$$\begin{aligned}\frac{\partial g_D}{\partial \boldsymbol{u}_{j_m}} =& \frac{\partial g_D}{\partial D_j}\sum_{i=1}^{n_{RF}}\left(c_{m_i}\frac{\partial D_{j_i}}{\partial \tilde{\sigma_{j_i}}}\left(\frac{\partial \tilde{\sigma}_j}{\partial \hat{\sigma}_{j_{mx}}}\frac{\partial \hat{\sigma}_{j_x}}{\partial \hat{\boldsymbol{u}}_j}+\right.\right. \\ & \left.\left.\frac{\partial \tilde{\sigma}_j}{\partial \hat{\sigma}_{j_{my}}}\frac{\partial \hat{\sigma}_{j_y}}{\partial \hat{\boldsymbol{u}}_j}\right)\right)\end{aligned} \tag{41}$$

Here the partial derivatives of the amplitude and mean stress components with respect to the reference displacements are constant in each iteration and calculated by:

$$\frac{\partial \hat{\boldsymbol{\sigma}}_j}{\partial \hat{\boldsymbol{u}}_j} = \begin{bmatrix} \frac{\partial \hat{\sigma}_{j_x}}{\partial \hat{\boldsymbol{u}}_j} \\ \frac{\partial \hat{\sigma}_{j_y}}{\partial \hat{\boldsymbol{u}}_j} \\ \frac{\partial \hat{\tau}_j}{\partial \hat{\boldsymbol{u}}_j} \end{bmatrix} = \tilde{x}_j(x)^q\boldsymbol{E}_j\boldsymbol{B}_j, \quad \forall j \tag{42}$$

Note that the constitutive matrix and strain-displacement matrix are constant and equal for all elements in this work.

As can be seen from the above equations, the additional computational costs as compared with stress constraints are the analysis and derivatives of Basquin's equation and Palmgren-Miner's equation, assuming that the computational cost of the Sines equivalent stress criterion is similar to a stress criterion. Furthermore, the equations that must be evaluated for each cycle *i* are either computational inexpensive or can be found by linear scaling. Consequently, the sensitivity analysis for fatigue constraints can be done very efficiently.

References

[1] M. P. Bendsøe and N. Kikuchi, "Generating optimal topologies in structural design using a homogenization method," *Computer Methods in Applied Mechanics and Engineering*, vol. 71, no. 2, pp. 197–224, nov 1988.

[2] M. P. Bendsøe, "Optimal shape design as a material distribution problem," *Structural optimization*, vol. 1, no. 4, pp. 193–202, 1989.

[3] M. Zhou and G. I. N. Rozvany, "The COC algorithm, Part II: Topological, geometrical and generalized shape optimization," *Computer Methods in Applied Mechanics and Engineering*, vol. 89, no. 1, pp. 309–336, 1991.

[4] M. P. Bendsøe and O. Sigmund, *Topology Optimization - Theory, Methods, and Applications*, 2nd ed. Springer-Verlag Berlin Heidelberg, 2004.

[5] O. Sigmund, "A 99 line topology optimization code written in Matlab," *Structural and Multidisciplinary Optimization*, vol. 21, no. 2, pp. 120–127, 2001.

[6] E. Andreassen, A. Clausen, M. Schevenels, B. Lazarov, and O. Sigmund, "Efficient topology optimization in MATLAB using 88 lines of code," *Structural and Multidisciplinary Optimization*, vol. 43, no. 1, pp. 1–16, 2011.

[7] M. P. Bendsøe and O. Sigmund, "Material interpolation schemes in topology optimization," *Archive of Applied Mechanics*, vol. 69, no. 9, pp. 635–654, 1999.

[8] W. S. Dorn, R. E. Gomory, and H. J. Greenberg, "Automatic design of optimal structures," *Journal de Mecanique*, vol. 3, pp. 25–52, 1964.

[9] G. Sved and Z. Ginos, "Structural optimization under multiple loading," *International Journal of Mechanical Sciences*, vol. 10, no. 10, pp. 803–805, oct 1968.

[10] U. Kirsch, "On singular topologies in optimum structural design," *Structural optimization*, vol. 2, no. 3, pp. 133–142, 1990.

[11] G. D. Cheng and X. Guo, "ϵ-relaxed approach in structural topology optimization," *Structural optimization*, vol. 13, no. 4, pp. 258–266, 1997.

[12] M. Bruggi, "On an alternative approach to stress constraints relaxation in topology optimization," *Structural and Multidisciplinary Optimization*, vol. 36, no. 2, pp. 125–141, 2008.

[13] C. Le, J. Norato, T. Bruns, C. Ha, and D. Tortorelli, "Stress-based topology optimization for continua," *Structural and Multidisciplinary Optimization*, vol. 41, no. 4, pp. 605–620, 2010.

[14] P. Duysinx and M. P. Bendsøe, "Topology optimization of continuum structures with local stress constraints," *International Journal for Numerical Methods in Engineering*, vol. 43, no. 8, pp. 1453–1478, 1998.

[15] M. Bruggi and P. Duysinx, "Topology optimization for minimum weight with compliance and stress constraints," *Structural and Multidisciplinary Optimization*, vol. 46, no. 3, pp. 369–384, 2012.

[16] G. Kreisselmeier and R. Steinhauser, "Systematic Control Design By Optimizing a Vector Performance Index," in *Computer Aided Design of Control Systems*, 1980, pp. 113–117.

[17] R. J. Yang and C. J. Chen, "Stress-based topology optimization," *Structural optimization*, vol. 12, no. 2, pp. 98–105, 1996.

[18] J. París, F. Navarrina, I. Colominas, and M. Casteleiro, "Topology optimization of continuum structures with local and global stress constraints," *Structural and Multidisciplinary Optimization*, vol. 39, no. 4, pp. 419–437, 2009.

[19] Y. Luo and Z. Kang, "Topology optimization of continuum structures with Drucker–Prager yield stress constraints," *Computers & Structures*, vol. 90, pp. 65–75, 2012.

[20] Y. Luo, M. Y. Wang, and Z. Kang, "An enhanced aggregation method for topology optimization with local stress constraints," *Computer Methods in Applied Mechanics and Engineering*, vol. 254, pp. 31–41, 2013.

[21] P. Duysinx and O. Sigmund, "New developments in handling stress constraints in optimal material distribution," *7th AIAA/USAF/NASA/ISSMO Symposium on Multidisciplinary Analysis and Optimization*, 1998.

[22] A. Verbart, M. Langelaar, and F. van Keulen, "A unified aggregation and relaxation approach for stress-constrained topology optimization," *Structural and Multidisciplinary Optimization*, vol. 55, no. 2, pp. 663–679, 2017.

[23] J. Grunwald and E. Schnack, "Modeling fatigue for shape optimization of dynamically loaded parts," *Advances in Engineering Software*, vol. 29, no. 1, pp. 63–67, 1998.

[24] M. Mrzyglod and A. P. Zielinski, "Numerial implementation of multiaxial high-cycle fatigue criterion to structural optimization," *Journal of Theoretical and Applied Mechanics*, vol. 44, no. 3, pp. 691–712, 2006.

[25] N. Kaya, d. Karen, and F. Öztürk, "Re-design of a failed clutch fork using topology and shape optimisation by the response surface method," *Materials & Design*, vol. 31, no. 6, pp. 3008–3014, 2010.

[26] K. Sherif, W. Witteveen, K. Puchner, and H. Irschik, "Efficient Topology Optimization of Large Dynamic Finite Element Systems Using Fatigue," *AIAA Journal*, vol. 48, no. 8, pp. 1339–1347, 2010.

[27] G. J. Park and B. S. Kang, "Validation of a Structural Optimization Algorithm Transforming Dynamic Loads into Equivalent Static Loads," *Journal of Optimization Theory and Applications*, vol. 118, no. 1, pp. 191–200, 2003.

[28] Y.-I. Kim and G.-J. Park, "Nonlinear dynamic response structural optimization using equivalent static loads," *Computer Methods in Applied Mechanics and Engineering*, vol. 199, no. 9, pp. 660–676, 2010.

[29] S. H. Jeong, D.-H. Choi, and G. H. Yoon, "Fatigue and static failure considerations using a topology optimization method," *Applied Mathematical Modelling*, vol. 39, no. 3, pp. 1137–1162, 2015.

[30] M. Collet, M. Bruggi, and P. Duysinx, "Topology optimization for minimum weight with compliance and simplified nominal stress constraints for fatigue resistance," *Structural and Multidisciplinary Optimization*, vol. 55, no. 3, pp. 839–855, 2017.

[31] E. Holmberg, B. Torstenfelt, and A. Klarbring, "Fatigue constrained topology optimization," *Structural and Multidisciplinary Optimization*, vol. 50, no. 2, pp. 207–219, 2014.

[32] E. Holmberg, "Stress and fatigue constrained topology optimization," Licentiate thesis No. 1571, Linköping University, 2013.

[33] J. Norato, C. Le, and C. Ha, "Fatigue-based topology optimization method and tool," *US Patent Application No. 13/692,268*, 2012.

[34] B. Bourdin, "Filters in topology optimization," *International Journal for Numerical Methods in Engineering*, vol. 50, no. 9, pp. 2143–2158, mar 2001.

[35] T. E. Bruns and D. A. Tortorelli, "Topology optimization of non-linear elastic structures and compliant mechanisms," *Computer Methods in Applied Mechanics and Engineering*, vol. 190, no. 26, pp. 3443–3459, 2001.

[36] A. Díaz and O. Sigmund, "Checkerboard patterns in layout optimization," *Structural optimization*, vol. 10, no. 1, pp. 40–45, 1995.

[37] C. S. Jog and R. B. Haber, "Stability of finite element models for distributed-parameter optimization and topology design," *Computer Methods in Applied Mechanics and Engineering*, vol. 130, no. 3, pp. 203–226, 1996.

[38] O. Sigmund and J. Petersson, "Numerical instabilities in topology optimization: A survey on procedures dealing with checkerboards, mesh-dependencies and local minima," *Structural optimization*, vol. 16, no. 1, pp. 68–75, 1998.

[39] J. París, F. Navarrina, I. Colominas, and M. Casteleiro, "Block aggregation of stress constraints in topology optimization of structures," *Advances in Engineering Software*, vol. 41, no. 3, pp. 433–441, 2010.

[40] E. Holmberg, B. Torstenfelt, and A. Klarbring, "Stress constrained topology optimization," *Structural and Multidisciplinary Optimization*, vol. 48, no. 1, pp. 33–47, 2013.

[41] G. Sines, "Behavior of Metals Under Complex Static and Alternating Stresses," *Metal Fatigue*, pp. 145–169, 1959.

[42] R. I. Stephens, A. Fatemi, R. R. Stephens, and H. O. Fuchs, *Metal Fatigue in Engineering*, 2nd ed., ser. A Wiley-Interscience publication. John Wiley & Sons, 2000.

[43] M. A. Akgün, R. T. Haftka, K. C. Wu, J. L. Walsh, and J. H. Garcelon, "Efficient structural optimization for multiple load cases using adjoint sensitivities," *AIAA Journal*, vol. 39, no. 3, pp. 511–516, 2001.

[44] J. Oest, R. Sørensen, L. C. T. Overgaard, and E. Lund, "Structural optimization with fatigue and ultimate limit constraints of jacket structures for large offshore wind turbines," *Structural and Multidisciplinary Optimization*, vol. 55, no. 3, pp. 779–793, 2017.

[45] K. Svanberg, "The method of moving asymptotes—a new method for structural optimization," *International Journal for Numerical Methods in Engineering*, vol. 24, no. 2, pp. 359–373, 1987.

[46] ——, "MMA and GCMMA - version September 2007," KTH, Stockholm, Sweden, Tech. Rep., 2007.